Stem Cell Reports
Article

ISSCR

OPEN ACCESS

Naked Mole Rat Cells Have a Stable Epigenome that Resists iPSC Reprogramming

Li Tan,[1,2,6] Zhonghe Ke,[1,6] Gregory Tombline,[1] Nicholas Macoretta,[1] Kevin Hayes,[1] Xiao Tian,[1] Ruitu Lv,[2] Julia Ablaeva,[1] Michael Gilbert,[1] Natarajan V. Bhanu,[3] Zuo-Fei Yuan,[3] Benjamin A. Garcia,[3] Yujiang G. Shi,[2,4] Yang Shi,[2,5] Andrei Seluanov,[1,*] and Vera Gorbunova[1,*]

[1]Department of Biology, University of Rochester, Rochester, NY 14627, USA
[2]Laboratory of Epigenetics, Institutes of Biomedical Sciences and Department of Cellular and Genetic Medicine, School of Basic Medical Sciences, Shanghai Medical College of Fudan University, Shanghai 200032, P. R. China
[3]Epigenetics Program, Department of Biochemistry and Biophysics, Perelman School of Medicine, University of Pennsylvania, Philadelphia, PA 19104, USA
[4]Division of Endocrinology, Diabetes and Hypertension, Brigham and Women's Hospital, Harvard Medical School, Boston, MA 02115, USA
[5]Division of Newborn Medicine, Boston Children's Hospital, Department of Cell Biology, Harvard Medical School, Boston, MA 02115, USA
[6]Co-first author
*Correspondence: andrei.seluanov@rochester.edu (A.S.), vera.gorbunova@rochester.edu (V.G.)
https://doi.org/10.1016/j.stemcr.2017.10.001

SUMMARY

Naked mole rat (NMR) is a valuable model for aging and cancer research due to its exceptional longevity and cancer resistance. We observed that the reprogramming efficiency of NMR fibroblasts in response to OSKM was drastically lower than that of mouse fibroblasts. Expression of SV40 LargeT antigen (LT) dramatically improved reprogramming of NMR fibroblasts. Inactivation of Rb alone, but not p53, was sufficient to improve reprogramming efficiency, suggesting that NMR chromatin may be refractory to reprogramming. Analysis of the global histone landscape revealed that NMR had higher levels of repressive H3K27 methylation marks and lower levels of activating H3K27 acetylation marks than mouse. ATAC-seq revealed that in NMR, promoters of reprogramming genes were more closed than mouse promoters, while expression of LT led to massive opening of the NMR promoters. These results suggest that NMR displays a more stable epigenome that resists de-differentiation, contributing to the cancer resistance and longevity of this species.

INTRODUCTION

Naked mole rat (NMR) is the longest-lived rodent species (Buffenstein, 2005) and is becoming a popular model in research due to its longevity and very low incidence of cancer (Delaney et al., 2013, 2016; Lewis et al., 2012). NMRs have mouse-like body size but display almost ten times longer maximum lifespan and tumor resistance as opposed to tumor-prone mice. This makes NMR-to-mouse comparison very informative for identifying mechanisms of longevity and cancer resistance. Several such mechanisms have already been identified. For instance, NMR cells secrete very-high-molecular-weight hyaluronan, which prevents malignant transformation (Tian et al., 2013). Furthermore, NMRs express a unique *INK4* isoform, pALT, which consists of the first exon of *p15INK4b* and the second and third exons of *p16INK4a* and confers more efficient growth arrest (Tian et al., 2015). NMR cells also have significantly higher translation fidelity than mouse cells (Azpurua et al., 2013) and display better protein stability and less age-associated increase in cysteine oxidation during aging (Perez et al., 2009). In addition, NMRs have markedly higher levels of cytoprotective NRF2 signaling activity due to the lower negative regulators of this signaling, such as Keap1 and βTrCP (Lewis et al., 2015). Finally, loss of either tumor suppressor p53 or Rb individually triggers apoptosis in NMR cells (Seluanov et al., 2009), and loss of the tumor suppressor ARF triggers cellular senescence (Miyawaki et al., 2016).

Chromatin undergoes dynamic, organizational changes over an organism's life and may be a contributing cause of aging. Indeed, aging is associated with loss of heterochromatin and smoothening of patterns of transcriptionally active and repressed chromatin regions (for review, see Benayoun et al., 2015). This is subsequently associated with loss of repressive histone marks and spreading of active histone marks, culminating in the "heterochromatin loss model of aging," according to which age-related chromatin loss and de-repression of silenced genes lead to aberrant gene expression patterns and cellular dysfunction (Tsurumi and Li, 2012).

Induced pluripotent stem cells (iPSCs) present a promising approach for regenerative medicine. However, tumorigenicity of these cells is a major concern for potential clinical applications (Ben-David and Benvenisty, 2011). Malignant transformation and cellular reprogramming share several characteristics such as changes in epigenetic marks, gene expression, and metabolic characteristics (Folmes et al., 2011; Suva et al., 2013). Furthermore, expression of the reprogramming genes *Oct4*, *Sox2*, *Klf4*, and *c-Myc* (OSKM) is frequently perturbed in cancer (Ben-David and Benvenisty, 2011; Suva et al., 2013). Epigenetic changes driven by OSKM play the key role in the reprograming process. Histone modifications, histone

variants, and chromatin remodeling enzymes involved in reprogramming have been the subject of intense investigation (Nashun et al., 2015). Reprograming requires erasure of the existing somatic epigenetic memory and the establishment of a new epigenetic signature (Nashun et al., 2015). Early reprogramming events are associated with widespread loss of H3K27me3 and opening of the chromatin (Hussein et al., 2014). Reprogramming also requires bivalent chromatin domains that have both activating H3K4me3 and repressive H3K27me3 marks. Furthermore, several factors can reduce the efficiency of reprogramming: H3K27me3 represses pluripotency-associated genes (Mansour et al., 2012), HP-1γ impedes reprogramming by maintaining heterochromatin (Sridharan et al., 2013), and downregulation of H2A.X completely inhibits reprogramming (Wu et al., 2014). Interestingly, H2A.X plays an important role in promoting reprogramming and controlling the differentiation potential of iPSCs, which is independent of its role in DNA damage sensing (Wu et al., 2014). Finally, DNA methylation resists reprogramming, and inhibiting the activity of DNMT1 has been reported to increase reprogramming efficiency (Mikkelsen et al., 2008).

Here, we report that NMR cells are highly resistant to OSKM reprogramming. The frequency of iPSCs colonies was extremely low and was enhanced by inactivating Rb protein using SV40 LT antigen (LT). The resulting iPSCs could be expanded *in vitro* and differentiated into the cell lineages of three germ layers *in vitro*. The frequency of teratoma formation *in vivo* was very low compared with mouse iPSCs. Comparison of the histone landscapes in NMR and mouse using mass spectrometry revealed higher levels of repressive marks and lower levels of activating marks in the NMR cells. Furthermore, bivalent promoters in the mouse cells were repressed in the NMR, and this repression was alleviated by LT. Assay for transposase-accessible chromatin with high-throughput sequencing (ATAC-seq) revealed that NMR had more closed chromatin at promoter regions, and LT led to a massive opening of promoters. All together, these findings suggest that NMR cells have a more stable epigenome that is resistant to OSKM reprogramming. This more stable epigenome may contribute to the cancer resistance and longevity of this unique rodent and may provide novel insights into cancer prevention and treatment in humans.

RESULTS

NMR Fibroblasts Are More Resistant to OSKM-Induced Reprogramming than Mouse Fibroblasts

To generate the NMR iPSCs, we co-transfected NMR embryonic fibroblasts (NEFs) at population doubling time (PD) 10 with pPB-CAG-OSKM expressing mouse OSKM factors and PBase expressing PiggyBac transposase. No alkaline-phosphatase-positive (AP+) iPS colonies were observed in NEF transfectants after 4 weeks of culture in naive culture conditions (FBS + Lif or N2B27 + Lif + 2i) on feeder layers (Figure 1A). In contrast and as a positive control, MEFs at a comparable PD number could be easily reprogrammed into AP+ iPSC colonies (Figure 1A). Similar results were also obtained in adult NMR skin fibroblasts (NSF) (Figure 1B). Importantly, transfection efficiency, measured by transfecting a GFP plasmid, was higher in NMR cells than in mouse cells (Figure S1A) and could not account for the low reprogramming efficiency of NMR cells. Since the above fibroblasts have been cultured *in vitro* for several passages, we also used freshly isolated fibroblasts for reprogramming. Although the freshly isolated skin fibroblasts underwent mesenchymal-epithelial transition at low frequency upon OSKM overexpression, these epithelial-like colonies (Figure S1B) stopped growth soon and could not be expanded in either mouse or human embryonic stem cell (ESC)/iPSC culture medium. Similarly, no iPS-like colonies were observed when we used human OSKM factors (Figure S1C).

Next, we attempted to reprogram the NMR fibroblasts under primed-type PSCs conditions (Miyawaki et al., 2016) (KSR + bFGF + 2i). Under these conditions, NMR cells gave rise to AP+ colonies, but the frequency of AP+ colonies was 10-fold lower than for mouse cells (Figures 1C, 1D, and S1D). In order to rule out the possibility of species specificity of OSKM factors, we cloned the NMR OSKM factors in pPB-CAG vector (Figure S1E) and reprogrammed the NMR fibroblasts. We observed no improvement in reprogramming efficiency relative to mouse OSKM factors (Figure S1F). Taken together, these results suggest that NMR fibroblasts are more resistant to OSKM-induced cellular reprogramming than mouse fibroblasts.

LT Rescues the Low Reprogramming Efficiency of NMR Fibroblasts

We speculated that OSKM might be insufficient to reprogram NMR somatic cells toward pluripotency. To address this problem, we used an OSKM + X strategy to screen for factor(s) that could facilitate the reprogramming of NMR fibroblasts (Figure 2A). Twelve additional factors that have been reported to improve the reprogramming efficiency in mouse or human fibroblasts (*Nanog*, *Lin28*, *Rar + Lrg*, *Hif1a*, *Dppa4*, *Dppa5*, *Sox15*, *hTERT*, *CEBPa*, *p53DD*, and *LT*) were screened in NSF and NEF cells by co-transfecting them with OSKM. Among the 12 factors, only LT restored the iPSC reprogramming (Figure 2B). LT is a viral oncoprotein that binds and inactivates both p53 and pRb. Importantly, the NMR iPS-like colonies generated by OSKM + LT (NMR OSKMLT iPSCs) could be expanded and maintained in the pluripotent state after passaging to

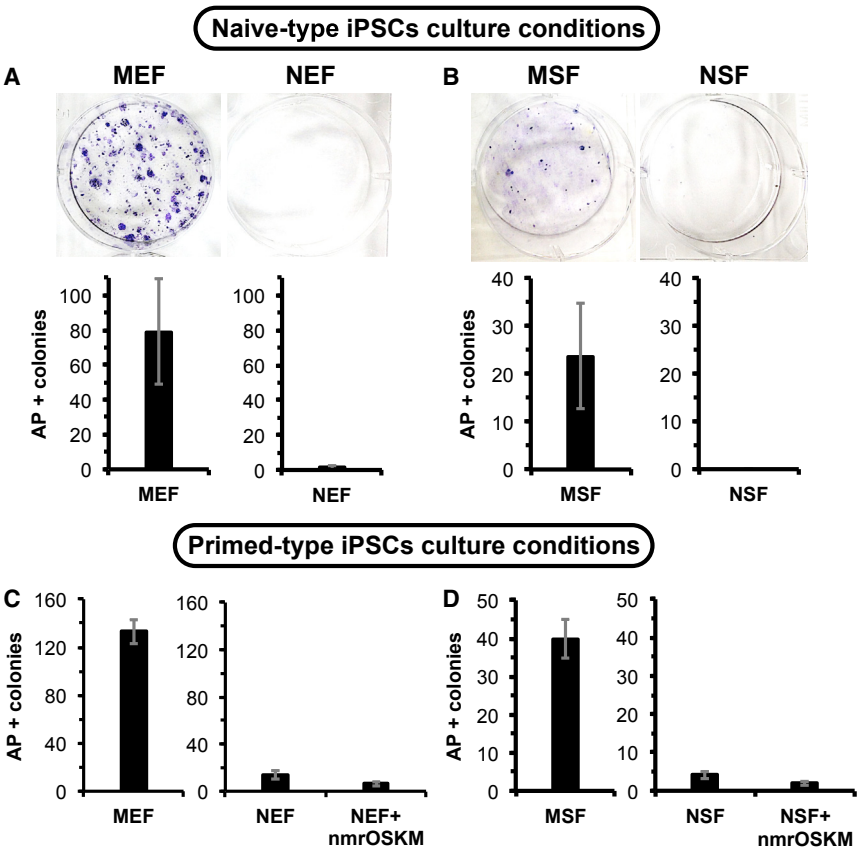

Figure 1. NMR Fibroblasts Are More Resistant to OSKM-Induced Cellular Reprogramming than Mouse Fibroblasts

(A) Representative AP staining of MEFs and NEFs upon mouse OSKM reprogramming under naive-type conditions (N2/B27 + LIF + 2i medium). NMR embryonic fibroblasts showed resistance to OSKM reprogramming. The graph below shows quantification of reprogramming efficiency (number of AP+ colonies per 10^5 transfected cells) of MEFs and NEFs.

(B) Representative AP staining of MSFs and NSFs upon mouse OSKM reprogramming under naive-type conditions (N2/B27 + LIF + 2i medium). NMR skin fibroblasts also showed resistance to OSKM reprogramming. The graph below shows the quantification of reprogramming efficiency (number of AP+ colonies per 10^5 transfected cells) of MSFs and NSFs.

(C) Quantification of iPSC reprogramming of embryonic fibroblasts under primed-type conditions (KSR + bFGF + 2i medium).

(D) Quantification of iPSC reprogramming of skin fibroblasts under primed-type conditions (KSR + bFGF + 2i medium).

All cell lines were at PD <10 at the start of reprogramming. The reprogramming was performed with mouse OSKM factors, unless otherwise indicated. The experiments were repeated at least five times, in two independent cell lines of each type, and error bars denote SD. MEF, mouse embryonic fibroblasts; NEF, naked mole rat embryonic fibroblasts; MSF, mouse skin fibroblasts; NSF, naked mole rat skin fibroblasts; nmrOSKM, reprogramming performed with naked mole rat OSKM factors.

new dishes (Figure 2C). This result indicates that either p53, pRb, or both pathways interfere with OSKM-induced cellular reprogramming in NMR fibroblasts. We also tested whether oxygen concentration may affect NMR reprogramming efficiency by performing reprogramming under physiological 3% O_2 and under ambient 20% O_2. Reprogramming efficiency for both species was higher at 3% O_2 (Figure S2A).

To determine whether the p53 or pRb pathway inhibits reprogramming of NMR cells, we used the mutant derivatives of LT; LTΔ434-444 inactivates pRb and its family members (p107 and p130), while LTK1 inactivates p53 (Hahn et al., 2002). Only LTΔ434-444 significantly increased the efficiency of OSKM reprogramming, under both naive and primed-type conditions (Figure 2D), and the resulting colonies could be expanded and maintained similarly to the colonies generated by the addition of the wild-type LT. It was reported that ARF suppression induces senescence in NMR fibroblasts (Miyawaki et al., 2016). As ARF suppression represses p53, we further tested whether p53 knockdown by LTK1 had a similar effect. We did not observe enlarged cells with senescent morphology or SA-β-gal positive cells after LTK1 transfection (Figure S2B), suggesting that senescence was not the reason for low reprogramming efficiency in LTK1-transfected cells. These results taken together indicate that the Rb pathway is responsible for the resistance of NMR cells to reprogramming.

Next, we compared the efficiencies of the p53 and Rb pathways in NMR and mouse cells, as these two pathways are known to be major barriers to reprogramming in mouse and human (Hong et al., 2009; Kawamura et al., 2009; Li et al., 2009; Marion et al., 2009; Utikal et al., 2009). A reporter containing a p53-binding site fused to firefly luciferase ORF showed stronger activation in mouse cells than in the NMR cells (Figure 2F). However, a reporter containing an E2F binding site showed stronger repression in the NMR cells than in the mouse cells (Figure 2G). These results were unlikely to be affected by sequence divergence between mouse and NMR, as the p53 DNA-binding domain and Rb showed very high similarity between NMR and mouse (88% and 91%, respectively). Furthermore,

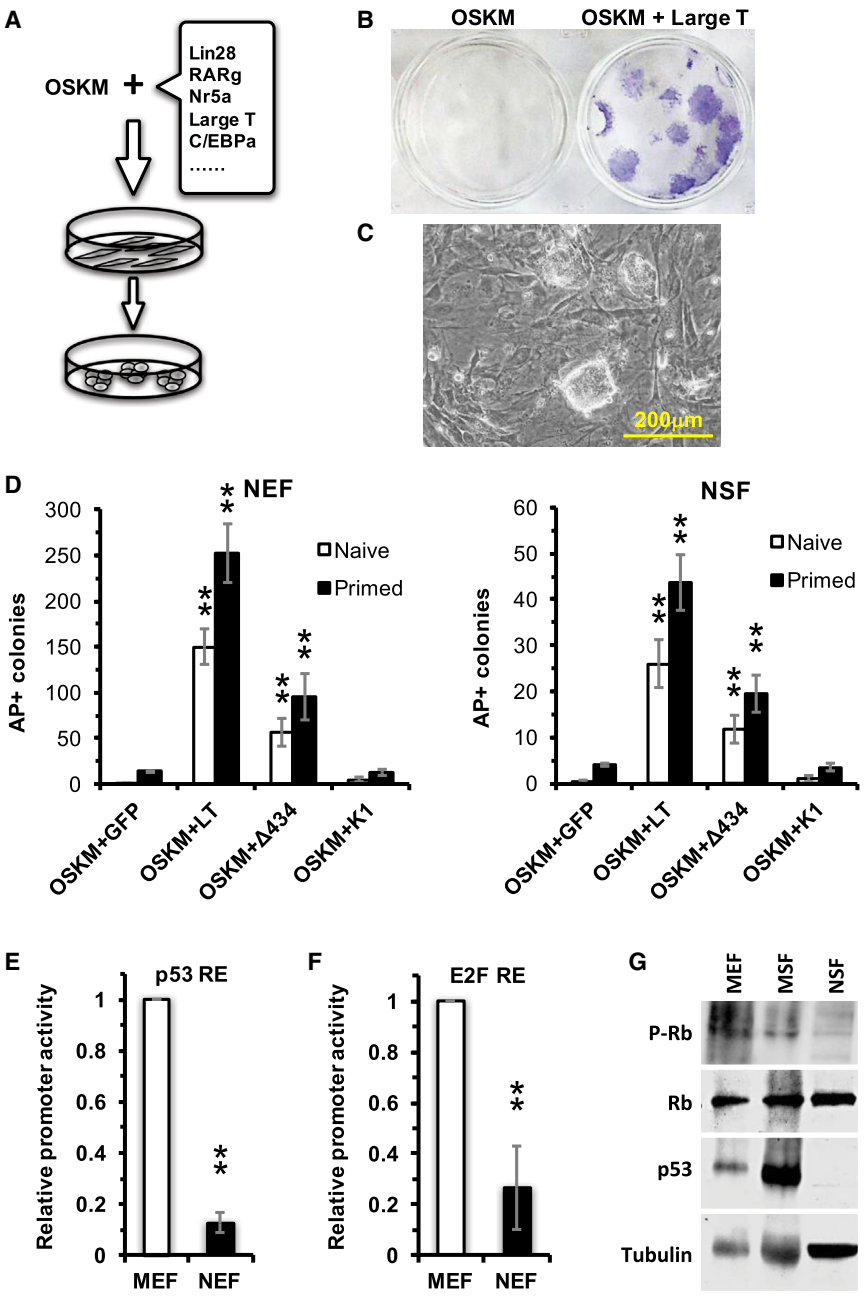

Figure 2. Overexpression of LT Facilitates OSKM-Induced Reprogramming of NMR Fibroblasts into iPSCs

(A) Diagram of the "OSKM + X" strategy for screening for factors than can facilitate the reprogramming of NMR fibroblasts into iPSCs. The 12 candidate genes that were tested are *Nanog*, *Lin28*, *Rar + Lrg*, *Hif1a*, *Dppa4*, *Dppa5*, *Sox15*, *hTERT*, *CEBPa*, *p53DD*, *SV40-LT*. Primers sequences used for subcloning can be found in Table S1.

(B) Among the 12 factors, only LT facilitated the formation of AP+ iPS-like colonies from NSFs (shown) or NEF cells. The cell lines were at PD <10 at the start of reprogramming.

(C) The "OSKM + LT" NSF iPSC colonies were expanded *in vitro*.

(D) LT promotes reprogramming of NMR cells by inactivating Rb. NMR fibroblasts (PD 8–16) were transfected with OSKM and either wild-type LT or its mutant derivatives, LTΔ434-444 (Δ434), which inactivates Rb, or LTK1 (K1), which inactivates p53. Reprogramming was performed under naive and primed conditions. The experiments were repeated three times and error bars denote SD. **p < 0.01.

(E) NEFs have lower basal p53 activity than MEFs. NSF cells were transfected with a reporter plasmid containing luciferase gene fused to p53 response element (p53 RE). p53 activity leads to promoter activation. The experiments were repeated three times and error bars denote SD. The cell lines were at PD <10. **p < 0.01.

(F) NEFs have higher basal Rb activity than MEFs. MEFs and NSFs (PD 8–16) were transfected with a reporter plasmid containing luciferase gene fused to E2F binding site (E2F RE). Rb activity represses the reporter. The experiments were repeated three times and error bars denote SD. The cell lines were at PD <10. **p < 0.01.

(G) Western blot showing that mouse cells have a higher level of p53 while NMR cells have a lower level of phosphorylated Rb. The cell lines were at PD <10.

Rb-associated transcription factors E2F and DP1 DNA-binding domains are identical between NMR and mouse (Figure S2C). Consistent with the luciferase assay results, NMR cells had higher levels of hypo-phosphorylated Rb, while mouse cells had higher levels of p53 (Figure 2G). Cumulatively, these results suggest that NMR cells have a more powerful Rb pathway, which serves as a barrier to OSKM reprogramming.

Characterization of NMR iPSCs

NMR OSKMLT iPSCs proliferated in culture for more than 1 year. Karyotypic analysis showed the iPSCs had normal karyotype (Figure S3). RT-qPCR analysis confirmed the activation of endogenous Oct-3/4, E-cadherin, and NANOG in NMR iPSCs (Figure 3A). Interestingly, *HAS2,* a gene encoding a hyaluronan synthase, was shut down in NMR OSKMLT iPSCs, consistent with our earlier observation

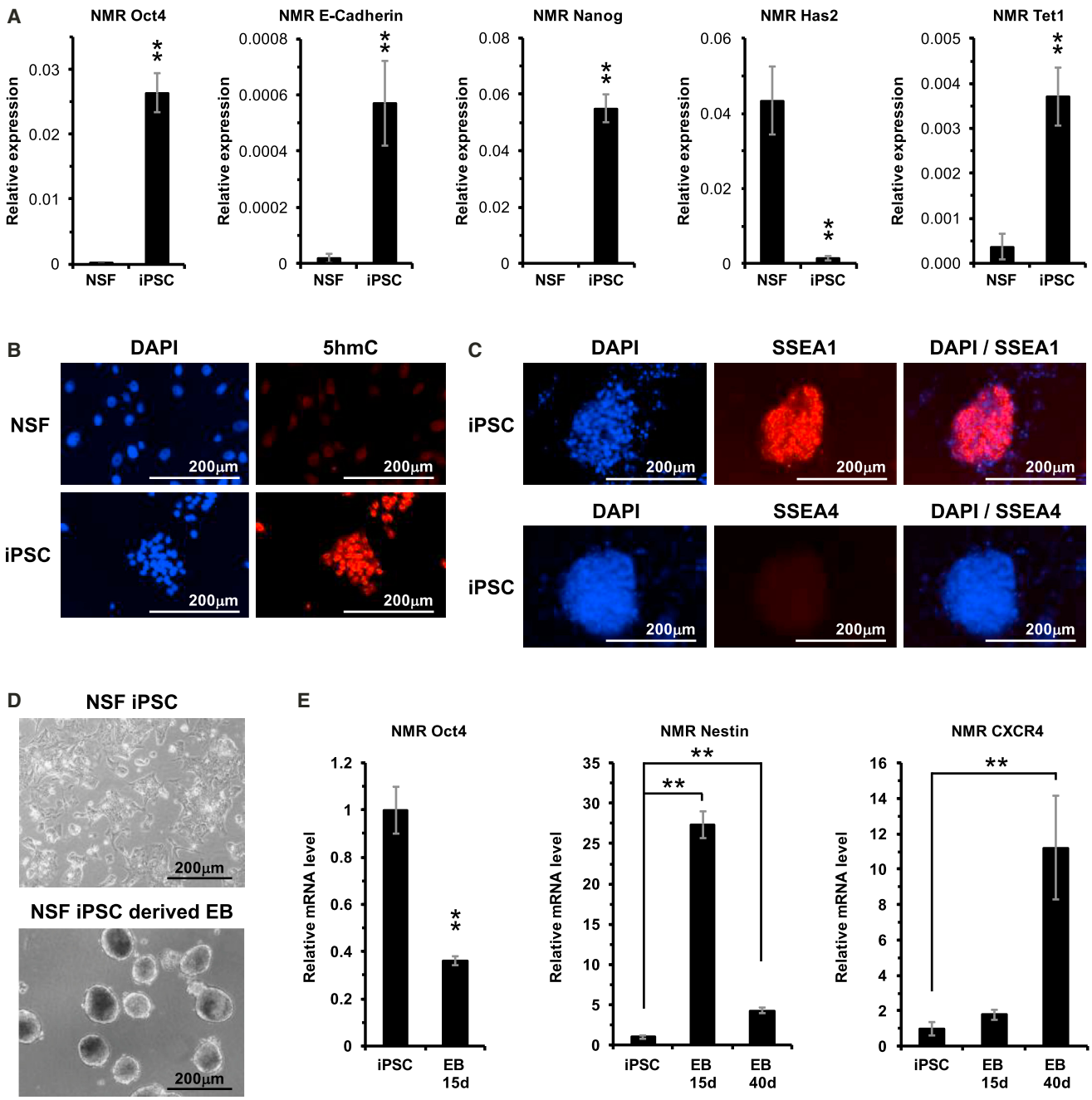

Figure 3. Characterization of NMR iPSCs

(A) RT-qPCR analysis of the expression of *Oct4*, *Nanog*, *E-Cadherin*, *Tet1*, and *HAS2* in NSFs and NSF-derived iPSCs. Primer sequences can be found in Table S2. The experiments were repeated three times and error bars denote SD. **p < 0.01.

(B) Immunostaining of 5hmC in NSF iPSCs. Images are taken at 200× magnification.

(C) Immunostaining of SSEA1, SSEA4 in NSF iPSCs. Images are taken at 200× magnification.

(D) Morphology of EBs derived from NSF iPSCs.

(E) Downregulation of pluripotent marker Oct4 and upregulation of ectoderm (Nestin) and mesoderm (CXCR4) during EB differentiation. The experiments were repeated three times and error bars denote SD. **p < 0.01.

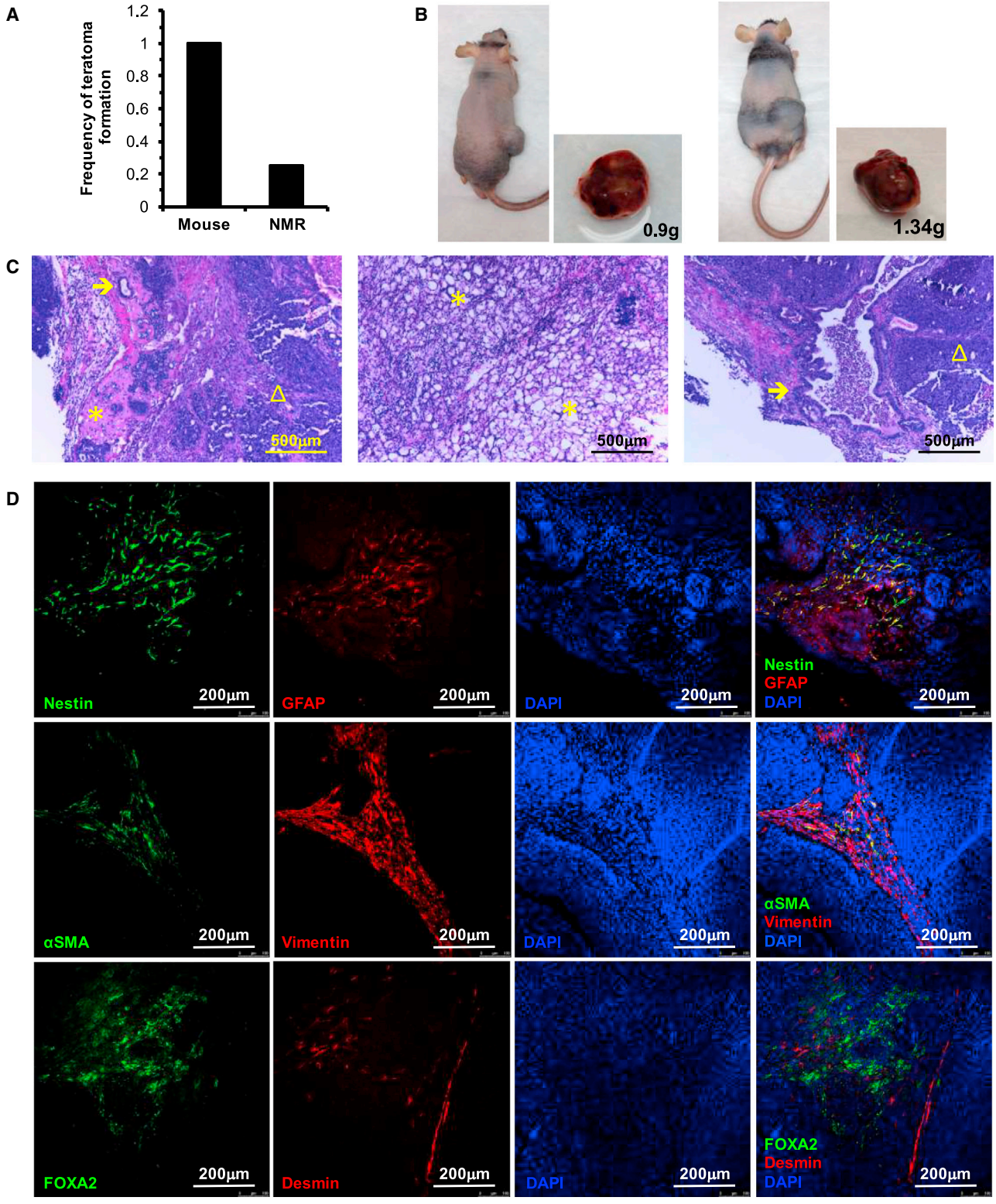

Figure 4. NMR iPSCs Form Teratoma in NUDE Mice

(A) Frequency of teratoma formation by NMR and mouse iPSCs. iPSCs (1×10^7 cells) were injected subcutaneously into immunodeficient mice. Ten mice were injected with MSF iPSCs and all formed teratomas; 16 mice were injected with NSF iPSCs and only four formed teratomas.

(legend continued on next page)

that NMR embryonic cells do not produce high-molecular-weight hyaluronan (Tian et al., 2013). TET1, a DNA oxidase that helps establish high 5hmC in mouse or human ESCs/iPSCs, was also activated in NMR iPSCs (Figure 3A). Consistently, 5hmC, the product of TET1-catalyzed 5mC oxidation, was present at higher levels in iPSCs (Figure 3B). Immunostaining showed that NMR iPSCs expressed the mouse pluripotent marker SSEA-1 but not the human pluripotent marker SSEA-4 (Figure 3C). Thus, our data suggest that the pluripotent network has been activated in our NMR iPSCs.

To verify the NMR iPSCs obtained under naive conditions display features of naive-type iPSCs, we checked X chromosome reactivation in female NMR iPSCs. The naive iPSCs retain a pre-inactivation X chromosome state and lack a silencing mark on the X chromosome in female iPSCs (Gafni et al., 2013). We found that the *Xist* RNA, a mark for X chromosome inactivation, was drastically reduced in NMR iPSCs derived from female NMR fibroblasts and cultured under naive-type conditions, while the iPSCs obtained under primed-type conditions retained *Xist* RNA expression (Figure S3B). Another X chromosome-linked gene, *Hprt1*, did not reduce its expression in naive-type iPSCs and showed about 2-fold higher level of expression compared with the primed-type iPSCs (Figure S3C) due to the dosage compensation effect of two active X chromosomes. This result showed that the NMR iPSCs cultured under naive conditions had one of the features of naive iPSCs. For brevity, we hereafter refer to these cells as naive-type iPSCs. However, additional characterization, such as comparison of expression of additional naive markers, not currently feasible in the NMR due to incomplete genome annotation, would be needed to definitively classify these cells as naive-type iPSCs.

We further evaluated the *in vitro* and *in vivo* differentiation capability of naive-type NMR iPSCs. NMR iPSCs formed embryoid body (EB) spheres in suspension culture (in an ultra-low attaching dish) (Figure 3D), and the differentiation markers of three germ layers were detected in the differentiating EB cultures (Figure 3E). Interestingly, NMR iPSCs were very inefficient at forming teratomas in immunodeficient mice. Out of 16 nude mice injected subcutaneously with NMR OSKMLT iPSCs, only four developed teratomas (Figures 4A and 4B), and the teratomas took 2–5 months to grow to detectable size. In contrast, mouse iPSCs formed teratomas in all injected mice, and the tumors developed within 3–4 weeks. Teratomas formed by NMR OSKMLT iPSCs displayed three germ layers that were verified with the following markers: GFAP and Nestin for ectoderm; αSMA and Desmin for mesoderm; Vimentin and FOXA2 for endoderm (Figure 4D). These results indicate that, although the NMR iPSCs have the capability to differentiate into three germ layers *in vitro* and *in vivo*, they exhibit additional tumor suppressor activities that restrict their tumorigenicity.

Naked Mole Rat Epigenome Is Enriched with Marks that Restrict Reprogramming

Since we found that inactivation of Rb enabled reprogramming of NMR iPSCs and Rb plays a major role in maintaining stable chromatin states independently of its role in cell-cycle control (Kareta et al., 2015), we hypothesized that NMR may have a more stable epigenome that is refractory to OSKM reprogramming. To test this hypothesis, we first compared chromatin states at the promoters of genes involved in reprogramming in the mouse and NMR using chromatin immunoprecipitation (ChIP)-qPCR. As previously reported (Hussein et al., 2014), the promoter of *E-cadherin* had bivalent chromatin marks in mouse fibroblasts, showing enrichment for both the permissive (H3K4me3) and the repressive (H3K27me3) histone marks. Such a bivalent chromatin organization is critical for reprogramming (Azuara et al., 2006; Bernstein et al., 2006). Strikingly, the *E-cadherin* promoter in NMR fibroblasts had only the repressive histone mark, H3K9me3 (Figure 5A). Introducing LT reduced the H3K9me3 modification on *E-cadherin* promoter. Similarly, *Utf1* gene (encoding Undifferentiated Embryonic Cell Transcription Factor 1) had bivalent chromatin marks in the mouse, but was repressed in the NMR. LT treatment increased the activating H3K4me3 mark on the *Utf1* promoter and reduced the repressing marks (Figure 5A). For another gene, *SSEA1* (*Fut4*), which was observed to be bivalent in the mouse and repressed in the NMR, LT treatment increased the levels of the activating H3K4me3 mark but did not significantly reduce the repressive marks (Figure 5A). Thus, introducing LT into NMR cells led to either opening of the repressed gene promoters or

(B) Representative tumor images of NSF iPSCs formed in nude mice; the tumors took an average of 3 months to grow to detectable size.
(C) Representative structures of three germ layers in the teratomas of NSF iPSCs. NSF iPSCs (1×10^7 cells) were injected subcutaneously in nude mice. Arrows indicate endodermal derivatives (gut-like); stars indicate mesodermal derivatives (bone-like and adipocyte-like structures); triangles indicate ectodermal derivatives (neuroepithelial-like structures).
(D) Immunofluorescence pictures of NSF iPSCs teratoma paraffin sections stained with three germ layer markers: Nestin (expressed in neuroectoderm) and GFAP (expressed in CNS) for the ectoderm layer; αSMA and Desmin (both expressed in muscle) for the mesoderm layer; FOXA2 (expressed in hepatocytes) and Vimentin (type III intermediate filament expressed in mesenchyme and fibroblasts) for the endoderm layer.

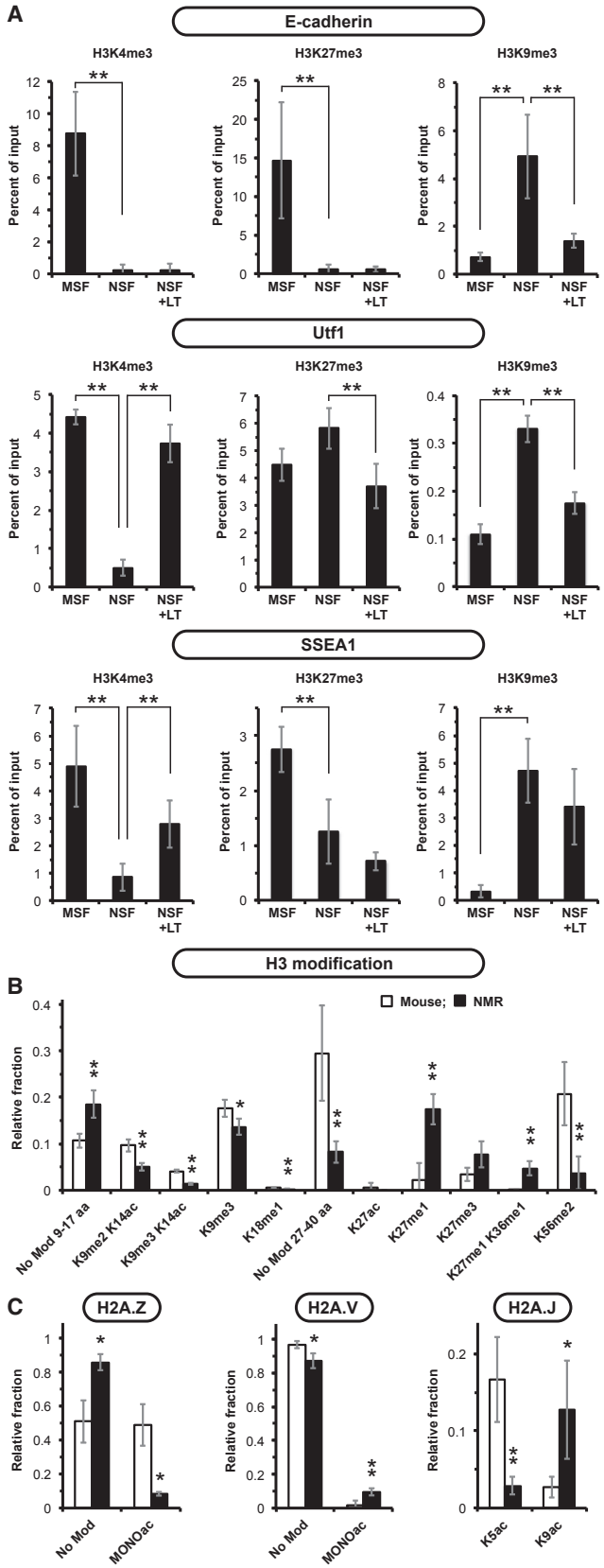

Figure 5. Comparison of Histone Posttranslational Modifications in NMR and Mouse Fibroblasts

(A) H3K4me3, H3K27me3, and H3K9me3 histone marks were analyzed by ChIP-qPCR on the promoters of E-cadherin, *Utf1*, and *SSAE1* (*Fut4*) genes in MSF and NSF cells. These genes have bivalent histone marka (H3K4me3+/H3K27me3+) in the mouse but show repressive marks in the NMR. This repression is partially alleviated by LT. Enrichment of each histone modification on the promoter was normalized to input DNA. Primer sequences can be found in Table S3. The experiments were repeated three times, and error bars represent SD. $^{**}p < 0.01$.

(B) Total histone H3 marks that significantly differ in abundance between NSFs and MSFs. The complete dataset of histone marks is shown in Table S4. The levels of H3 marks were determined by quantitative mass spectrometry in three independent lines of NSFs and MSFs. MSFs had higher levels of H3K9 methylation marks associated with heterochromatin, typical of mouse cells (Figure S4), while NSFs had higher levels of H3K27 methylation marks associated with silencing of gene regions. The relative fraction of a specific mark was calculated by dividing the abundance of the specific mark by the sum of all forms of the same given peptide, which was considered as 1. Error bars indicate SD. $^{**}p < 0.01$, $^{*}p < 0.05$. For K27me3, the p value was 0.058; K27ac peptide was undetectable in the NSFs, therefore no p value is provided.

(C) Histone H2A variants show differences in acetylation marks. The levels of H2A acetylation marks were determined by quantitative mass spectrometry in three independent lines of NSFs and MSFs. Error bars indicate SD. $^{**}p < 0.01$, $^{*}p < 0.05$. Data on other histone modifications that did not show statistically significant differences are shown in Table S4. All cells used in the experiments described in this figure were at PD <10.

changing chromatin marks into the bivalent form. Analysis of additional promoters in the NMR was complicated by the lack of accurately mapped transcription start sites in the NMR genome.

Next, we compared global histone landscapes in the NMR and mouse using quantitative mass spectrometry. Relative abundance of histone posttranslational modifications (PTMs) was determined in three lines of mouse fibroblasts and four lines of NMR fibroblasts where each line was derived from an individual animal. The complete dataset of relative abundances of histone PTMs is available in Table S4, whereas the PTMs showing significant differences between NMR and mouse are discussed below. The levels of unmodified H3 K9-14 peptide were higher in the NMR than in the mouse. Furthermore, NMR cells had lower levels of H3K9me3, H3K9me2K14ac, and H3K9me3K14ac peptides than the mouse cells (Figure 5B). In contrast, the levels of unmodified H3K27-40 peptide were lower in the NMR than in the mouse. NMR cells had lower levels of H3K27ac and higher levels of H3K27me1, H3K27me3, and H3K27me1K36me1 peptides. NMR cells also had lower H3K56me2 (Figure 5B). H3K9 and H3K56 methylation marks correspond to heterochromatin. Mouse cells are

A

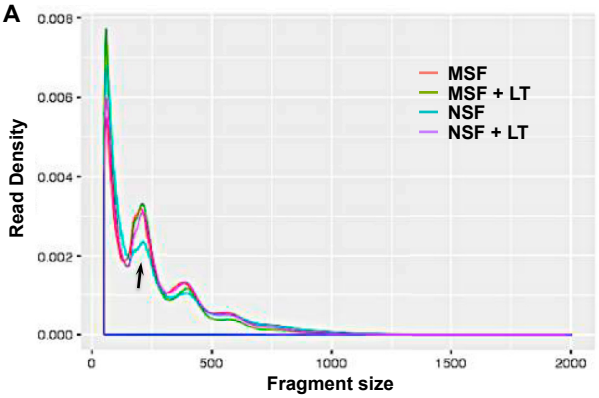

B

Name	Number of peaks	Peaks in promoters	Genes with peaks
MSF	75,120	13,543	14,436
MSF+LT	63,258	13,318	14,164
NSF	80,661	11,737	12,404
NSF+LT	83,297	12,199	12,895

C

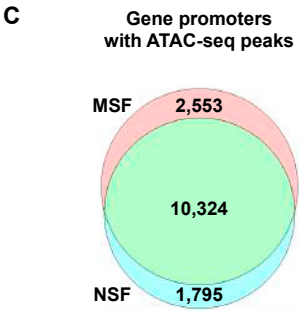

D

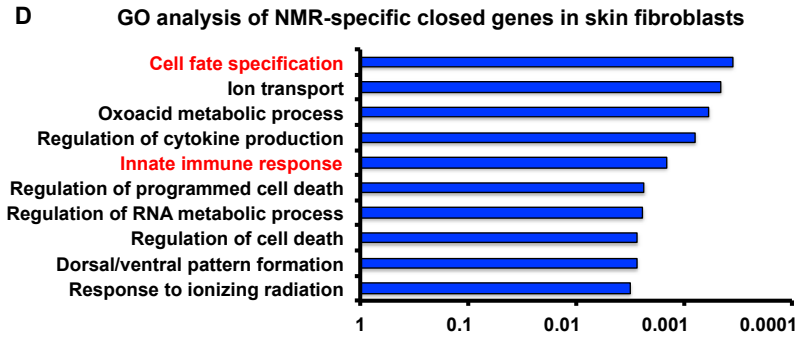

E

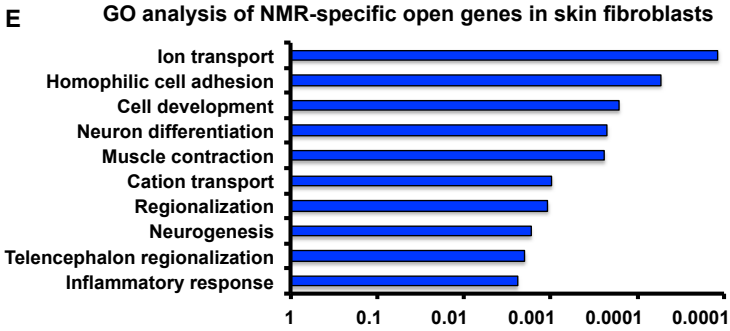

F

ATAC peaks	Whole genome	Promoter region
Gain MSF	8,367	547
Loss MSF	15,137	509
Gain NSF	21,344	2,873
Loss NSF	21,869	874

G

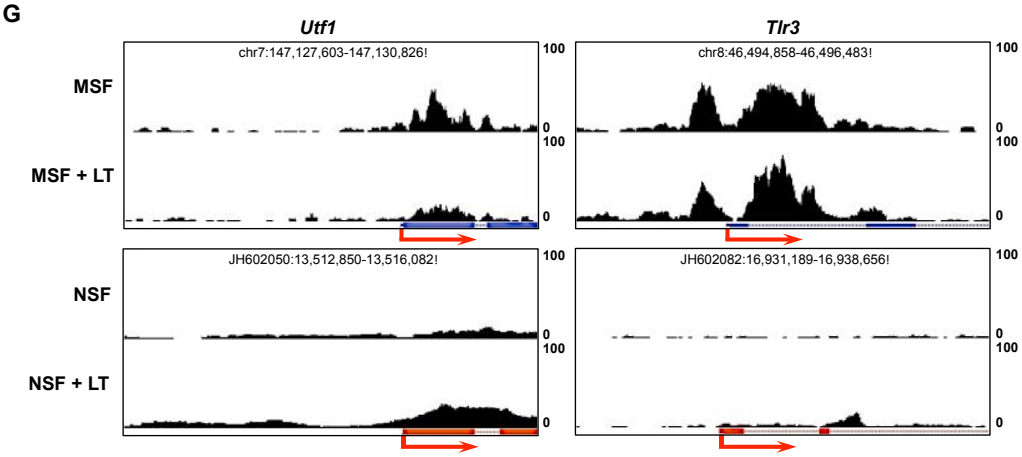

(legend on next page)

known to have large heterochromatic regions that are visible by *in situ* staining. Interestingly, NMR cells had no such heterochromatin foci (Figure S4). This may explain the higher levels of PTMs associated with constitutive heterochromatin in mouse cells, which is unlikely to affect reprogramming. In contrast, H3K27 methylation is associated with silencing of differentiation-related genes and pluripotency genes (Bernstein et al., 2006; Hammoud et al., 2009; Mochizuki et al., 2012). Furthermore, H3K27me3 was reported to repress pluripotency-associated genes (Mansour et al., 2012) and higher levels of this modification can make cells refractory to reprogramming.

Unmodified histone variant H2A.Z was more abundant in the NMR, while the acetylated form of H2A.Z was more abundant in the mouse (Figure 5C). H2A.Z is enriched on gene promoters (Barski et al., 2007). The unmodified H2A.Z is associated with repression while the acetylated form is associated with active transcription (Marques et al., 2010). H2A.Z acetylation is also associated with epigenetic deregulation during carcinogenesis (Valdes-Mora et al., 2012), suggesting that lower levels of H2A.Z acetylation in the NMR may prevent cell reprogramming and malignant transformation. Histone H2 variants H2A.V and H2A.J also showed differential acetylation between mouse and NMR (Figure 5C), however, the biological roles of these histones are not well understood.

We next compared epigenetic landscapes in NMR and mouse using ATAC-seq in NMR and mouse fibroblasts with and without LT. ATAC-seq quantifies open chromatin regions genome wide (Buenrostro et al., 2015). Fragment lengths corresponding to single nucleosomes were underrepresented in the NMR relative to the mouse, while LT removed this difference, making NMR fragment lengths similar to that of the mouse (Figure 6A). The lower levels of single-nucleosome fragments may suggest that in the NMR, the chromatin is enriched for regions that are more open as well as for regions that are more compact than in the mouse, with fewer regions in the "intermediate" single-nucleosome state. The total number of peaks corresponding to open chromatin was higher in the NMR (Figure 6B), which could be explained by the lower numbers of repetitive elements in the NMR genome (Kim et al., 2011). However, the number of accessible regions within the promoters was higher in the mouse (Figure 6B), indicating that NMR has more closed chromatin in gene regions. Moreover, gene ontology (GO) analysis showed that the genes with ATAC-seq peak(s) in MSF but not in NSF are enriched in GO items: "cell fate specification" and "innate immune response" associated with cellular reprogramming (Lee et al., 2012) (Figures 5C–5E). Upon LT expression, mouse cells lost almost twice as many peaks as they gained, while NMR cells lost and gained a similar number of peaks genome wide (Figure 6F). Remarkably, in the promoter regions, mouse cells gained 547 peaks and lost 509 peaks, while NMR cells gained 2,873 peaks and lost 874 peaks (Figure 6F). This result shows that LT triggered massive opening of gene promoters in the NMR but not in the mouse cells. The promoter peaks opened by LT in NMR cells corresponded to 1,163 genes; 520 of these genes were also NMR-specific

Figure 6. ATAC-Seq Analysis of NMR and Mouse Epigenetic Landscapes

(A) Fragment length distribution in the ATAC-seq library. ATAC-seq was performed on NSFs, MSFs, and corresponding cell lines expressing LT (NSF-LT and MSF-LT). The small fragments represent sequence reads in open chromatin, while the peak indicated by an arrow results from sequence reads that span one nucleosome; larger peaks represent progressively more compact chromatin.

(B) NSFs have more open chromatin globally but the promoters are less open. To compare genes with ATAC-seq peaks in two different species, we annotated peaks to genes first and then compared the gene lists with or without ATAC peaks between MSFs and NSFs. The number of open chromatin regions (ATAC-seq peaks) is greater in the NSFs than in MEFs. LT leads to a greater number of peaks in the NSFs but fewer peaks in the MSFs. In the promoter regions, NSFs have fewer peaks than MSFs, and LT increases the number of peaks in NSFs but not in MSFs.

(C) Venn diagram overlap between open gene promoters (promoters with ATAC-seq peaks) in MSFs and NSFs.

(D) GO analysis of the genes with opened chromatin in the mouse but closed in the NMR (NMR-specific closed genes in skin fibroblasts). Two terms marked in red font have been reported to be associated with reprogramming. Venn diagrams of the genes opened by LT are shown in Figure S3.

(E) GO analysis of the genes with opened chromatin in NSFs but closed in MSFs.

(F) Effect of LT on peak gain and loss in the NSFs and MSFs. To quantitatively identify the differential ATAC peaks in the same species with or without LT, the ATAC peaks with more than 2-fold difference in density between two samples were defined as "gain" or "loss" ATAC peaks in cells upon LT overexpression. It should be noted that those weak peaks in which the differential values between two samples were less than 10 reads/bp have been removed to eliminate false positives. LT expression results in a greater number of peaks lost in the mouse cells than in the NSFs genome wide. In promoter regions, a similar number of peaks are lost and gained by the MSFs, while in the NSFs, LT leads to massive opening of chromatin with over 3-fold more peaks gained than lost.

(G) Representative gene loci (*Utf1* and *Tlr3*) with ATAC-seq peaks in MSF but not in NSFs. LT overexpression opened the chromatin of these gene loci in NSFs.

All cells used in the experiments described in this figure were at PD <10.

closed genes, i.e., these genes were open in mouse cells even without LT (Figures S5A and S5B). This group included genes implicated in reprogramming such as *Utf1*, *Tlr3* (Figure 6G), *SSEA1* (*Fut4*), and E-cadherin (*Cdh1*) (Figure S6). Cumulatively, these results suggest that the chromatin structure of gene promoter regions (including many genes essential for cellular reprogramming) in the NMR fibroblasts is more closed than in the mouse fibroblasts. Introducing LT into NMR cells opened the chromatin at promoter regions, bringing the number of peaks to the level found in mouse cells. Thus ATAC-seq analysis indicates that NMR cells have a less permissive chromatin state than mouse cells.

DISCUSSION

The comparison of the reprogramming process of NMR and mouse fibroblasts revealed several unexpected findings. NMR fibroblasts were refractory to OSKM-induced reprogramming in comparison with mouse fibroblasts. The AP+ colonies were formed at very low frequency and could not be expanded in the mouse iPSC/ESC culture medium. This was observed with both mouse and human OSKM factors under both naive and primed conditions. Similarly, while this study was in preparation, the very low efficiency of reprogramming was reported for NMR cells by Miyawaki et al. (2016) using human iPSC/ESC culture medium. Resistance of NMR cells to reprogramming is also being reported by our colleagues in an accompanying paper in this issue of *Stem Cell Reports* (Lee et al., 2017).

To understand the mechanism responsible for the resistance of NMR cells to reprogramming, we screened for factors that improve reprogramming efficiency. Our screen identified that SV 40 Large T antigen strongly improved NMR reprograming efficiency, albeit the resulting LT NMR iPSCs colonies still proliferated slower than mouse iPSCs. The LT NMR iPSCs expressed pluripotent marker genes and could differentiate into the cell lineages of three germ layers *in vitro* and *in vivo*.

A unique feature of NMR iPSCs was the low efficiency in teratoma formation. This observation is consistent with NMR cancer resistance. Our previous work showed that NMR adult fibroblasts secrete high-molecular-weight hyaluronic acid, which protects cells from malignant transformation, and NMR fibroblasts expressing hRasV12, LT, and knockdown of the *HAS2* gene responsible for the synthesis of high-molecular-weight hyaluronic acid formed tumors in nude mice (Tian et al., 2013). However, *HAS2* was silenced in NMR iPSCs and the knockdown of *HAS2* had no significant effect on reprogramming of NSFs, suggesting that an additional mechanism is responsible for the low teratoma formation of NMR iPSCs. The recently published study by Miyawaki et al. (2016) also reported that NMR iPSCs did not form teratomas *in vivo* unless they expressed mouse ERas and shRNA to inhibit *Arf*.

In our study, NMR iPSCs formed teratomas, but the efficiency was low and the tumors grew very slowly. It is possible that we observed teratoma formation because our iPSCs contained LT and the efficiency of tumor formation would be improved by overexpressing mouse ERas or human RasV12, as in our previous study (Tian et al., 2013). Cumulatively, these results suggest that once NMR cells are reprogrammed into iPSCs, they require forced expression of Ras and inactivation of p53 or Rb pathways to form tumors *in vivo*. However, this does not explain the low reprogramming efficiency of NMR cells.

To understand how LT facilitates NMR cell reprogramming, we utilized the separation of its function mutations in our reprogramming assays (Hahn et al., 2002). LT is a viral oncoprotein that binds and inactivates two tumor suppressor genes, Rb and p53. Using mutated versions of LT, we showed that inactivation of Rb alone was sufficient to allow reprogramming of NMR cells. Furthermore, NMR fibroblasts displayed stronger basal Rb activity than mouse fibroblasts and much lower p53 basal activity than mouse fibroblasts. An ideal balance between p53 and Rb activities may vary between different species of mammals. For example, mouse cells are known to rely more heavily on p53 while human cells rely more on Rb (Gorbunova and Seluanov, 2010; Li et al., 2009). This may reflect the choice between reliance on elimination of damaged cells by apoptosis in the case of activating p53 versus reliance on cell-cycle arrest and heterochromatin repressive functions in the case of Rb. Our previous work showed that Rb had a stronger tumor suppressive function than p53 in NMR cells, and NMR fibroblasts expressing RasV12, combined with the knockdown of Rb and enzymatic degradation of hyaluronan, formed colonies in soft agar, while the cells expressing RasV12, combined with p53 and enzymatic degradation of hyaluronan, did not (Tian et al., 2013). Cumulatively, these results demonstrate that highly active Rb is a barrier to malignant transformation and reprogramming of NMR cells.

Cell reprogramming depends on changes in chromatin structure that erase histone marks of a differentiated cell and establish new marks of a pluripotent cell (Nashun et al., 2015). Rb guards against reprogramming in mouse fibroblasts through the silencing of *Sox2* as well as other pluripotent marker genes by maintaining a more repressive chromatin state (Kareta et al., 2015). Therefore, we hypothesized that NMR cells may have a more stable epigenome, and our quantitative mass spectrometry results are consistent with this hypothesis. Specifically, our analysis revealed that repressive H3K9 and H3K56-methylated

histones associated with constitutive heterochromatin were more abundant in the mouse, while methylated H3K27 associated with repression of developmental and reprogramming gene promoters was more abundant in the NMR. Mouse cells have large regions of constitutive heterochromatin that apparently do not affect reprograming efficiency but may carry the abundant H3K9 and H3K56 methylation marks. In contrast, NMR cells do not show prominent heterochromatic foci but carry higher levels of H3K27 methylation marks on gene promoters. H3K27 methylation was shown to repress pluripotency genes and counteract reprogramming (Zhao et al., 2013). Moreover, NMR cells had lower levels of permissive H2A.Z acetylation mark. The H2A.Z histone variant is generally associated with transcribed genes and H2A.Z acetylation promotes transcription while unmodified H2A.Z is repressive (Bonisch and Hake, 2012). The picture that emerged from histone PTM analysis was that mouse cells contain more abundant marks of constitutive heterochromatin and more abundant marks associated with active transcription of euchromatic regions. The NMR cells, on the contrary, have fewer marks of constitutive heterochromatin but more repressive marks at gene promoters.

Consistently, ChIP analysis of E-cadherin promoter involved in reprogramming showed that this promoter was bivalent in the mouse fibroblasts but contained only repressive marks in the NMR. Introducing LT reduced the levels of repressive marks on E-cadherin promoter.

We have also carried out ATAC-seq, and the results were very consistent with the histone PTM analysis. The total NMR genome has a higher number of ATAC-seq peaks, suggesting more open chromatin. This is consistent with the fact that NMR cells lack large regions of constitutive heterochromatin in the NMR cells. The NMR genome is smaller and contains fewer repetitive elements than the mouse genome (Kim et al., 2011). Repetitive elements may comprise a significant portion of constitutive heterochromatin found in mouse cells and carry abundant H3K9 and H3K56 methylation marks. Strikingly, the comparison of chromatin accessibility in promoter regions revealed that NMR cells had more closed chromatin at promoters than mouse cells. This result is again consistent with histone PTM analysis, which showed more abundant repressive H3K27 methylation marks in the NMR. This less accessible chromatin at promoters may impede reprogramming of the NMR cells. Remarkably, LT greatly increased the number of accessible promoter regions in the NMR, making it similar to that of the mouse genome, suggesting that LT enables NMR cell reprogramming by conferring a more permissive chromatin state.

Epigenetic regulation has been proposed to be an important player during aging (Benayoun et al., 2015; Booth and Brunet, 2016) and tumorigenesis (Liu et al., 2016; Soshnev et al., 2016). Cancer is associated with cellular de-differentiation and loss of tissue-specific histone marks. Aging also involves smoothening of the existing epigenetic patterns and loss of heterochromatin. Human progeroid syndromes, Werner and Hutchison-Gilford progeria, are both associated with loss of heterochromatin marks (Shumaker et al., 2006; Zhang et al., 2015). This, combined with similar observations in model organisms, led to the "global heterochromatin loss theory of aging" (Tsurumi and Li, 2012). If epigenetic stability is a key determinant of longevity and tumor suppression, long-lived and cancer-resistant species would be expected to be more epigenetically stable. Our comparison of the epigenetic landscapes and reprogramming efficiency between NMR and mouse fibroblasts strongly suggests that the somatic cells derived from the long-lived and cancer-resistant NMRs have a more stable epigenome than cells from short-lived and cancer-prone mice. Our work provides evidence that epigenomic stability is associated with longevity and cancer resistance in a wild-type organism. The study of a naturally long-lived and cancer-resistant NMR may provide clues to engineering more stable epigenomes to prevent cancer and extend the human lifespan.

EXPERIMENTAL PROCEDURES

Detailed experimental procedures, including cell culture, plasmids, cellular reprogramming, western blotting, karyotyping, culture of NMR iPSCs, alkaline phosphatase staining, luciferase assay, animal care and teratoma assays, immunostaining, RT-qPCR, ChIP-qPCR, mass spectrometry of histones, and ATAC-seq are provided in the Supplemental Information. All animal experiments were approved by the University of Rochester Institutional Animal Care and Use Committee.

SUPPLEMENTAL INFORMATION

Supplemental Information includes Supplemental Experimental Procedures, six figures, and four tables and can be found with this article online at https://doi.org/10.1016/j.stemcr.2017.10.001.

AUTHOR CONTRIBUTIONS

L.T., Z.K., X.T., G.T., Y.G.S., Y.S., A.S., and V.G. designed the research; L.T. performed all experiments on iPSC reprogramming and ChIP-qPCR analysis; Z.K. performed teratoma assays and immunohistochemistry; N.M. performed NMR OSKM cloning; K.H. assisted with immunofluorescence; J.A. assisted with cell culture; G.T., M.G., N.V.B., Z.-F.Y., and B.A.G. performed mass spectrometry analysis of histones; R.L. performed bioinformatics analysis of ATAC-seq data. L.T., Z.K., G.T., N.V.B, Z.-F.Y., B.A.G., A.S., and V.G. analyzed data; L.T., A.S., and V.G. wrote the manuscript.

ACKNOWLEDGMENTS

We thank Dr. Allan Bradley, Pengtao Liu, and Jian Yang in the Sanger Institute for providing the PiggyBac transpon system and Dr. Yi Zhang (URMC) for providing the CEBP-alpha plasmid. The authors also appreciate members of the Gorbunova and Seluanov labs for technical assistance (Lauren Wiener) and critical discussion (Michael Van Meter, Li Xie, Lingfeng Luo, Sarallah Rezazadeh). This work was supported by NIH grants GM110174 and CA196539 to B.G.; AG047200, AG027237, AG051449, and AG046320 to V.G. and A.S.; and Life Extension Foundation grants to V.G. and A.S. L.T. was partly supported by NSFC (31200966) and the Shanghai Pujiang Talent Program (16PJ1401500).

Received: August 8, 2016
Revised: September 29, 2017
Accepted: October 2, 2017
Published: October 26, 2017

REFERENCES

Azpurua, J., Ke, Z., Chen, I.X., Zhang, Q., Ermolenko, D.N., Zhang, Z.D., Gorbunova, V., and Seluanov, A. (2013). Naked mole-rat has increased translational fidelity compared with the mouse, as well as a unique 28S ribosomal RNA cleavage. Proc. Natl. Acad. Sci. USA *110*, 17350–17355.

Azuara, V., Perry, P., Sauer, S., Spivakov, M., Jorgensen, H.F., John, R.M., Gouti, M., Casanova, M., Warnes, G., Merkenschlager, M., et al. (2006). Chromatin signatures of pluripotent cell lines. Nat. Cell Biol. *8*, 532–538.

Barski, A., Cuddapah, S., Cui, K., Roh, T.Y., Schones, D.E., Wang, Z., Wei, G., Chepelev, I., and Zhao, K. (2007). High-resolution profiling of histone methylations in the human genome. Cell *129*, 823–837.

Ben-David, U., and Benvenisty, N. (2011). The tumorigenicity of human embryonic and induced pluripotent stem cells. Nat. Rev. Cancer *11*, 268–277.

Benayoun, B.A., Pollina, E.A., and Brunet, A. (2015). Epigenetic regulation of ageing: linking environmental inputs to genomic stability. Nat. Rev. Mol. Cell Biol. *16*, 593–610.

Bernstein, B.E., Mikkelsen, T.S., Xie, X., Kamal, M., Huebert, D.J., Cuff, J., Fry, B., Meissner, A., Wernig, M., Plath, K., et al. (2006). A bivalent chromatin structure marks key developmental genes in embryonic stem cells. Cell *125*, 315–326.

Bonisch, C., and Hake, S.B. (2012). Histone H2A variants in nucleosomes and chromatin: more or less stable? Nucleic Acids Res. *40*, 10719–10741.

Booth, L.N., and Brunet, A. (2016). The aging epigenome. Mol. Cell *62*, 728–744.

Buenrostro, J.D., Wu, B., Chang, H.Y., and Greenleaf, W.J. (2015). ATAC-seq: a method for assaying chromatin accessibility genome-wide. Curr. Protoc. Mol. Biol. *109*, 21–29.

Buffenstein, R. (2005). The naked mole-rat: a new long-living model for human aging research. J. Gerontol. A Biol. Sci. Med. Sci. *60*, 1369–1377.

Delaney, M.A., Nagy, L., Kinsel, M.J., and Treuting, P.M. (2013). Spontaneous histologic lesions of the adult naked mole rat (*Heterocephalus glaber*): a retrospective survey of lesions in a zoo population. Vet. Pathol. *50*, 607–621.

Delaney, M.A., Ward, J.M., Walsh, T.F., Chinnadurai, S.K., Kerns, K., Kinsel, M.J., and Treuting, P.M. (2016). Initial case reports of cancer in naked mole-rats (*Heterocephalus glaber*). Vet. Pathol. *53*, 691–696.

Folmes, C.D., Nelson, T.J., Martinez-Fernandez, A., Arrell, D.K., Lindor, J.Z., Dzeja, P.P., Ikeda, Y., Perez-Terzic, C., and Terzic, A. (2011). Somatic oxidative bioenergetics transitions into pluripotency-dependent glycolysis to facilitate nuclear reprogramming. Cell Metab. *14*, 264–271.

Gafni, O., Weinberger, L., Mansour, A.A., Manor, Y.S., Chomsky, E., Ben-Yosef, D., Kalma, Y., Viukov, S., Maza, I., Zviran, A., et al. (2013). Derivation of novel human ground state naive pluripotent stem cells. Nature *504*, 282–286.

Gorbunova, V., and Seluanov, A. (2010). A comparison of senescence in mouse and human cells. In Cellular Senescence and Tumor Suppression, P. Adams and J. Sedivy, eds. (Springer-Verlag), pp. 175–197.

Hahn, W.C., Dessain, S.K., Brooks, M.W., King, J.E., Elenbaas, B., Sabatini, D.M., DeCaprio, J.A., and Weinberg, R.A. (2002). Enumeration of the simian virus 40 early region elements necessary for human cell transformation. Mol. Cell. Biol. *22*, 2111–2123.

Hammoud, S.S., Nix, D.A., Zhang, H., Purwar, J., Carrell, D.T., and Cairns, B.R. (2009). Distinctive chromatin in human sperm packages genes for embryo development. Nature *460*, 473–478.

Hong, H., Takahashi, K., Ichisaka, T., Aoi, T., Kanagawa, O., Nakagawa, M., Okita, K., and Yamanaka, S. (2009). Suppression of induced pluripotent stem cell generation by the p53-p21 pathway. Nature *460*, 1132–1135.

Hussein, S.M., Puri, M.C., Tonge, P.D., Benevento, M., Corso, A.J., Clancy, J.L., Mosbergen, R., Li, M., Lee, D.S., Cloonan, N., et al. (2014). Genome-wide characterization of the routes to pluripotency. Nature *516*, 198–206.

Kareta, M.S., Gorges, L.L., Hafeez, S., Benayoun, B.A., Marro, S., Zmoos, A.F., Cecchini, M.J., Spacek, D., Batista, L.F., O'Brien, M., et al. (2015). Inhibition of pluripotency networks by the Rb tumor suppressor restricts reprogramming and tumorigenesis. Cell Stem Cell *16*, 39–50.

Kawamura, T., Suzuki, J., Wang, Y.V., Menendez, S., Morera, L.B., Raya, A., Wahl, G.M., and Izpisua Belmonte, J.C. (2009). Linking the p53 tumour suppressor pathway to somatic cell reprogramming. Nature *460*, 1140–1144.

Kim, E.B., Fang, X., Fushan, A.A., Huang, Z., Lobanov, A.V., Han, L., Marino, S.M., Sun, X., Turanov, A.A., Yang, P., et al. (2011). Genome sequencing reveals insights into physiology and longevity of the naked mole rat. Nature *479*, 223–227.

Lee, J., Sayed, N., Hunter, A., Au, K.F., Wong, W.H., Mocarski, E.S., Pera, R.R., Yakubov, E., and Cooke, J.P. (2012). Activation of innate immunity is required for efficient nuclear reprogramming. Cell *151*, 547–558.

Lee, S.-G., Mikhalchenko, A.E., Yim, S.H., Lobanov, A.V., Park, J.-K., Choi, K.-H., Bronson, R.T., Lee, C.-K., Park, T.J., and Gladyshev,

V.N. (2017). Naked mole rat induced pluripotent stem cells and their contribution to interspecific chimera. Stem Cell Reports *9*, this issue, 1706–1720.

Lewis, K.N., Andziak, B., Yang, T., and Buffenstein, R. (2012). The naked mole-rat response to oxidative stress: just deal with it. Antioxid. Redox Signal. *19*, 1388–1399.

Lewis, K.N., Wason, E., Edrey, Y.H., Kristan, D.M., Nevo, E., and Buffenstein, R. (2015). Regulation of Nrf2 signaling and longevity in naturally long-lived rodents. Proc. Natl. Acad. Sci. USA *112*, 3722–3727.

Li, H., Collado, M., Villasante, A., Strati, K., Ortega, S., Canamero, M., Blasco, M.A., and Serrano, M. (2009). The Ink4/Arf locus is a barrier for iPS cell reprogramming. Nature *460*, 1136–1139.

Liu, F., Wang, L., Perna, F., and Nimer, S.D. (2016). Beyond transcription factors: how oncogenic signalling reshapes the epigenetic landscape. Nat. Rev. Cancer *16*, 359–372.

Mansour, A.A., Gafni, O., Weinberger, L., Zviran, A., Ayyash, M., Rais, Y., Krupalnik, V., Zerbib, M., Amann-Zalcenstein, D., Maza, I., et al. (2012). The H3K27 demethylase Utx regulates somatic and germ cell epigenetic reprogramming. Nature *488*, 409–413.

Marion, R.M., Strati, K., Li, H., Murga, M., Blanco, R., Ortega, S., Fernandez-Capetillo, O., Serrano, M., and Blasco, M.A. (2009). A p53-mediated DNA damage response limits reprogramming to ensure iPS cell genomic integrity. Nature *460*, 1149–1153.

Marques, M., Laflamme, L., Gervais, A.L., and Gaudreau, L. (2010). Reconciling the positive and negative roles of histone H2A.Z in gene transcription. Epigenetics *5*, 267–272.

Mikkelsen, T.S., Hanna, J., Zhang, X., Ku, M., Wernig, M., Schorderet, P., Bernstein, B.E., Jaenisch, R., Lander, E.S., and Meissner, A. (2008). Dissecting direct reprogramming through integrative genomic analysis. Nature *454*, 49–55.

Miyawaki, S., Kawamura, Y., Oiwa, Y., Shimizu, A., Hachiya, T., Bono, H., Koya, I., Okada, Y., Kimura, T., Tsuchiya, Y., et al. (2016). Tumour resistance in induced pluripotent stem cells derived from naked mole-rats. Nat. Commun. *7*, 11471.

Mochizuki, K., Tachibana, M., Saitou, M., Tokitake, Y., and Matsui, Y. (2012). Implication of DNA demethylation and bivalent histone modification for selective gene regulation in mouse primordial germ cells. PLoS One *7*, e46036.

Nashun, B., Hill, P.W., and Hajkova, P. (2015). Reprogramming of cell fate: epigenetic memory and the erasure of memories past. EMBO J. *34*, 1296–1308.

Perez, V.I., Buffenstein, R., Masamsetti, V., Leonard, S., Salmon, A.B., Mele, J., Andziak, B., Yang, T., Edrey, Y., Friguet, B., et al. (2009). Protein stability and resistance to oxidative stress are determinants of longevity in the longest-living rodent, the naked mole-rat. Proc. Natl. Acad. Sci. USA *106*, 3059–3064.

Seluanov, A., Hine, C., Azpurua, J., Feigenson, M., Bozzella, M., Mao, Z., Catania, K.C., and Gorbunova, V. (2009). Hypersensitivity to contact inhibition provides a clue to cancer resistance of naked mole-rat. Proc. Natl. Acad. Sci. USA *106*, 19352–19357.

Shumaker, D.K., Dechat, T., Kohlmaier, A., Adam, S.A., Bozovsky, M.R., Erdos, M.R., Eriksson, M., Goldman, A.E., Khuon, S., Collins, F.S., et al. (2006). Mutant nuclear lamin A leads to progressive alterations of epigenetic control in premature aging. Proc. Natl. Acad. Sci. USA *103*, 8703–8708.

Soshnev, A.A., Josefowicz, S.Z., and Allis, C.D. (2016). Greater than the sum of parts: complexity of the dynamic epigenome. Mol. Cell *62*, 681–694.

Sridharan, R., Gonzales-Cope, M., Chronis, C., Bonora, G., McKee, R., Huang, C., Patel, S., Lopez, D., Mishra, N., Pellegrini, M., et al. (2013). Proteomic and genomic approaches reveal critical functions of H3K9 methylation and heterochromatin protein-1gamma in reprogramming to pluripotency. Nat. Cell Biol. *15*, 872–882.

Suva, M.L., Riggi, N., and Bernstein, B.E. (2013). Epigenetic reprogramming in cancer. Science *339*, 1567–1570.

Tian, X., Azpurua, J., Hine, C., Vaidya, A., Myakishev-Rempel, M., Ablaeva, J., Mao, Z., Nevo, E., Gorbunova, V., and Seluanov, A. (2013). High-molecular-mass hyaluronan mediates the cancer resistance of the naked mole rat. Nature *499*, 346–349.

Tian, X., Azpurua, J., Ke, Z., Augereau, A., Zhang, Z.D., Vijg, J., Gladyshev, V.N., Gorbunova, V., and Seluanov, A. (2015). INK4 locus of the tumor-resistant rodent, the naked mole rat, expresses a functional p15/p16 hybrid isoform. Proc. Natl. Acad. Sci. USA *112*, 1053–1058.

Tsurumi, A., and Li, W.X. (2012). Global heterochromatin loss: a unifying theory of aging? Epigenetics *7*, 680–688.

Utikal, J., Polo, J.M., Stadtfeld, M., Maherali, N., Kulalert, W., Walsh, R.M., Khalil, A., Rheinwald, J.G., and Hochedlinger, K. (2009). Immortalization eliminates a roadblock during cellular reprogramming into iPS cells. Nature *460*, 1145–1148.

Valdes-Mora, F., Song, J.Z., Statham, A.L., Strbenac, D., Robinson, M.D., Nair, S.S., Patterson, K.I., Tremethick, D.J., Stirzaker, C., and Clark, S.J. (2012). Acetylation of H2A.Z is a key epigenetic modification associated with gene deregulation and epigenetic remodeling in cancer. Genome Res. *22*, 307–321.

Wu, T., Liu, Y., Wen, D., Tseng, Z., Tahmasian, M., Zhong, M., Rafii, S., Stadtfeld, M., Hochedlinger, K., and Xiao, A. (2014). Histone variant H2A.X deposition pattern serves as a functional epigenetic mark for distinguishing the developmental potentials of iPSCs. Cell Stem Cell *15*, 281–294.

Zhang, W., Li, J., Suzuki, K., Qu, J., Wang, P., Zhou, J., Liu, X., Ren, R., Xu, X., Ocampo, A., et al. (2015). Aging stem cells. A Werner syndrome stem cell model unveils heterochromatin alterations as a driver of human aging. Science *348*, 1160–1163.

Zhao, W., Li, Q., Ayers, S., Gu, Y., Shi, Z., Zhu, Q., Chen, Y., Wang, H.Y., and Wang, R.F. (2013). Jmjd3 inhibits reprogramming by upregulating expression of INK4a/Arf and targeting PHF20 for ubiquitination. Cell *152*, 1037–1050.